International Journal of Engineering

Journal Homepage: www.ije.ir

Enhancing Fault Detection in Image Analysis: A Combined Wavelet-Fourier Technique for Advancing Manufacturing Quality Control

Z. Khodadadi[a], M. S. Owlia[*a], A. Amiri[b]

[a] *Department of Industrial Engineering, Yazd University, Yazd, Iran*
[b] *Department of Industrial Engineering, Shahed University, Tehran, Iran*

PAPER INFO

Paper history:
Received 27 August 2023
Received in revised form 27 September 2023
Accepted 02 October 2023

Keywords:
Quality Performance
Imaging Technologies
Feature Extraction
Statistical Process Control
Online Process Monitoring
Wavelet-Fourier Method
Fault Detection and Localization

ABSTRACT

This study focuses on utilizing image data for statistical process control and improving quality monitoring in manufacturing and service systems. The effectiveness of individual and combined feature extraction methods is evaluated, with the Wavelet-Fourier approach identified as the most suitable. The proposed method not only identifies image processing issues but also provides valuable information for estimating change points, fault locations, and fault sizes. This enables the resolution and prediction of faults, leading to cost and time savings in production. To perform evaluation of the proposed method, an image from a tile production line is subjected to Wavelet transform, followed by Fourier transform on the obtained coefficients. The results demonstrate the superiority of the Wavelet-Fourier method over individual methods such as Fourier transform and Wavelet transform. The proposed method exhibits comparable or improved performance in fault detection and localization compared to similar research. This study highlights the potential of utilizing image data for statistical process control and quality monitoring, offering a comprehensive solution for fault detection and analysis. The findings contribute to advancements in image processing techniques and have practical implications for enhancing quality monitoring in various industries. By leveraging image data, manufacturers can make informed decisions, enhance process performance, and improve overall product quality.

***doi**: 10.5829/ije.2024.37.02b.14*

Graphical Abstract

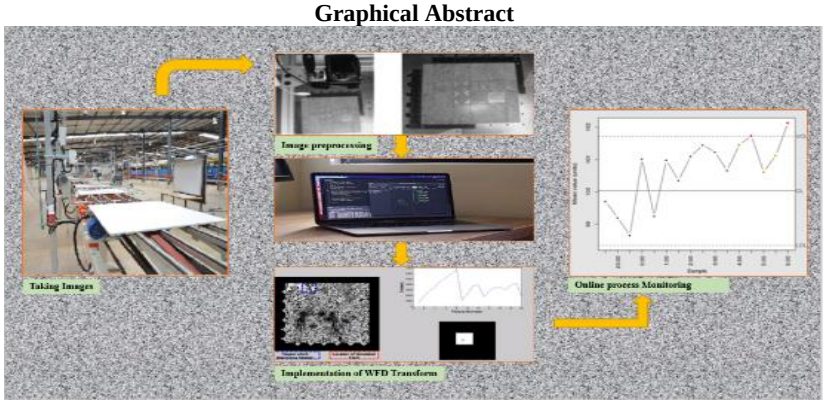

1. INTRODUCTION

In contemporary manufacturing and service industries, ensuring product reliability and customer satisfaction hinges on the successful implementation of robust quality control measures throughout production processes. The deployment of image analysis tools has proven invaluable in the detection of faults and defects across a wide spectrum of industries (1).

*Corresponding Author Email: owliams@yazd.ac.ir (M. S. Owlia)

Please cite this article as: Khodadadi Z, Owlia MS, Amiri A. Enhancing Fault Detection in Image Analysis: A Combined Wavelet-Fourier Technique for Advancing Manufacturing Quality Control, International Journal of Engineering, Transactions B: Applications. 2024;37(02):387-401.

The direct utilization of images within the domain of statistical process control, while promising, introduces its own set of challenges. These challenges encompass increased computational complexity and the vulnerability of features to variations. As the number of features derived from images grows, so does the computational burden, potentially impeding the model's ability to discern intricate relationships within high-dimensional data. Furthermore, the raw data extracted from images can be highly sensitive to even minor parameter fluctuations, affecting pixel values and potentially undermining the model's accuracy and reliability.

Image processing entails the conversion of an input image into a measurable or descriptive index as output, relying on the computation of a sequence of general or specific characteristics. In this process, the initial step involves capturing an image of the subject or object of interest. Subsequent analysis of these images necessitates the use of various computer facilities and software tools. Finally, by crafting suitable algorithms, a model is developed with the capacity to predict the current or future state of the target based on the extracted image features.

Descriptors, serving as representations of image quality aligned with human perception, facilitate effective image retrieval by similarity. While the Fourier transform has been widely employed for image description, it falls short in terms of resolution properties. Conversely, the Fourier descriptor demonstrates enhanced accuracy, efficiency, and performance in recovery and classification. This method allows for precise matching, ease of implementation, and sensitivity to low levels of noise. An increasingly popular alternative is the wavelet transform, which amalgamates the time and frequency domains, combining the advantages of both approaches. The wavelet transform dissects signals into fundamental functions, providing multi-scale image analysis. The fusion of wavelets with Fourier transforms enables a comprehensive examination of both the time and frequency domains.

Traditional methods of image analysis that exclusively leverage Fourier or wavelet transforms have displayed potential in the identification of specific fault types (2). Nevertheless, these techniques grapple with limitations when striving to accurately capture intricate variations or isolated anomalies. This research endeavor introduces a strategy that harnesses the complementary attributes of the wavelet and Fourier methods to address these constraints. Our proposed approach seeks to enhance the representation of image features and augment the distinction between authentic product variations and potential defects. It does so by uniting the multi-resolution analysis capabilities of the wavelet transform with the frequency domain analysis prowess of the Fourier transform. Through this integrated methodology, our study endeavors to significantly bolster the fault detection capabilities of image analysis systems employed in manufacturing quality control.

This transformation has been widely used in image processing and pattern classification, as demonstrated by Zahn (3) in their analysis of closed curves of aircraft using Fourier descriptors based on similarity between curves. The wavelet transform can improve the Fourier transform by enabling simultaneous analysis of signal information in both time and frequency domains; thus, enhancing the ability to capture local signal characteristics quickly. Chen (4) utilized a polar coordinate pattern (h, r) with the center of pattern mass as the origin. They then applied the Fourier transform along the polar angle axis h, and the wavelet transform along the r axis, resulting in extracted features that are invariant to translation, rotation, and scaling. This method was applied to a database of 85 items, and the results showed that the Fourier-Wavelet representation provided better information. Liu (5) proposed a alternative machine vision approach for quantitatively estimating and monitoring the appearance and aesthetics of manufactured products. The approach includes three main steps: (a) wavelet-based textural feature extraction from product images, (b) estimation of measures of product appearance through subspace projection of texture features, and (c) monitoring of the appearance in the latent variable subspace of textural features. Yadav et al. (6) conducted experiments on retrieval and classification of image-based objects using three techniques: Fourier Descriptor (FD), General Fourier Descriptor (GFD), and Fourier-Wavelet Descriptor (WFD). Classification results were compared among all three techniques, and it was found that WFD performed better than FD and GFD techniques The authors propose a method that integrates wavelet analysis and Fourier analysis to enhance the detection and diagnosis of quality issues in manufacturing systems. The technique is applied to a case study in the automotive industry, demonstrating its effectiveness in identifying and resolving quality problems. Hosntalab et al. (7) propose a multi-stage technique to classify teeth in multi-slice CT (MSCT) images. The proposed algorithm consists of the following three stages: segmentation, feature extraction and classification. The employed WFD approach was successful to discriminate and numbering of the teeth in the presence of missing teeth. Münch et al. (8) presented a fast, powerful and stable filter based on combined wavelet and Fourier analysis for the elimination of horizontal or vertical stripes in images and compared with other types of destriping filters. Strict separation between artifacts and original features allowing both, suppression of the unwanted structures and high degree of preservation of the original image information is endeavoured. The results are validated by visual assessments, as well as by quantitative estimation of the

image energy loss. Ward et al. (9) discusses the importance of maintaining the accuracy and completeness of in-formation conveyed through visual analytics, as well as the impact of data filtering, sampling, and other transformations on the decision-making process. Megahed et al. (10) propose a new spatiotemporal method for monitoring image data that considers spatial and temporal information. According to the type and purpose of image monitoring in this research, which is to monitor the tile production process, two types of image monitoring conditions have been used: uniformity and comparison with a specific pattern. Chen et al. (11) proposed a method for EEG seizure detection by decomposing EEG signals for up to six wavelet scales without downsampling. Experiments demonstrate that the proposed method is comparable and sometimes better than our previous dual-tree complex wavelet- Fourier method for the University of Bonn EEG database. Knešaurek (12) proposed an improved brain image capture technique using a combined Fourier-wavelet approach. The study results showed that the quality and quantification of 3D brain images can be significantly improved by using the Fourier-wavelet approach com-pared to the original images. Xia et al. (13) compares the effectiveness of wavelet and Fourier transforms for feature extraction in image analysis. The results show that the Wavelet-Fourier method outperforms the individual transforms, demonstrating its potential for enhancing image analysis tasks. Al-Salman et al. (14) proposed a statistical model and Fourier-wavelet analysis for detecting dukes. Ten properties were extracted and used in a method to identify sleep spindles, achieving accuracy, sensitivity, and diagnosis rates of 97.9%, 98.98%, and 97.8% with a window size of 0.5 seconds. You et al. (15) proposed a combined Fourier-Wavelet approach for dynamic analytical solutions. Wavelet transform effectively solves the inverse Fourier transform in physical problem-solving, benefiting flexible multilayer structures and risk management in civil engineering. According to Biglari et al. (16), a combined feature selection technique significantly reduces the number of features with only a slight decrease in prediction accuracy. Fattahzadeh and Saghaei (17) explored the application of video and satellite sensors for process monitoring, emphasizing the need for sequential images to detect complex process changes. They proposed a statistical approach using RIDGE regression and a Q control chart to monitor processes with temporal correlations and high-dimensional data, applicable to both color and gray images. Experimental results, compared to existing methods, demonstrate the method's effectiveness in detecting process changes. Santosh and Barpanda (18) developed an alternative method for glaucoma classification using wavelet-based PCA and enhanced retinal images. The method achieved highly satisfactory results in glaucoma diagnosis and classification. Abdul-Kareem and Al-Jawher (19) developed a new medical image encoding technique by combining discrete wavelet transform, fast Fourier transform, Arnold transform and two multidimensional chaotic systems. The proposed algorithm utilized two real-value transformations: the Discrete Fourier Transform (DFT), which generates real and imaginary coefficients, and the Discrete Wavelet Transform (DWT), which produces four sub-bands, which posed a significant challenge in retrieving images following the encoding and decoding procedure.

The literature review has illuminated the substantial contributions of the Wavelet-Fourier transform. As we move forward in this research, it is evident that the Wavelet-Fourier approach stands as a powerful tool for feature extraction, particularly in the context of image-based quality monitoring and statistical process control.

The research in this field has shown remarkable advancements in the detection and characterization of defects, anomalies, and patterns in data, leading to enhanced performance, reliability, and efficiency in numerous applications. One area of society that greatly benefits from the combined wavelet-Fourier technique is manufacturing. By utilizing this approach, companies are able to detect and diagnose faults or quality issues in their production processes more efficiently and accurately. This helps minimize waste, reduce costs, and improve overall product quality, ultimately leading to customer satisfaction and a competitive edge in the market. Additionally, further investigation into the optimization of the combined wavelet-Fourier technique for real-time applications would be valuable. As technology advances, there is an increasing demand for efficient and rapid data analysis.

Our research primarily aims to address a significant challenge in industrial quality control: the improvement of fault detection in image analysis. To tackle this challenge, we introduce an innovative combined technique, the Wavelet-Fourier method, designed to overcome the limitations associated with individual methods. This novel approach shows great promise in enhancing the identification and classification of defects, ultimately leading to enhanced efficiency and precision within quality control processes in manufacturing industries. By extracting valuable information from images, we empower the use of this data in control charts, allowing proactive measures to prevent and resolve process-related issues. Our study applies the Wavelet-Fourier method to analyze tile images acquired from the production line, using the results for informed decision-making during production and real-time monitoring of the production line. Subsequent sections delve into the feature extraction methods employed and comprehensively discuss the advantages inherent to the Wavelet-Fourier approach. Our research findings, obtained through simulation, robustly affirm the efficacy

of our proposed method, illustrating its potential as a valuable tool for image analysis and quality control spanning diverse industries. The subsequent sections describe the feature extraction methods utilized and comprehensively discuss the advantages associated with the Wavelet-Fourier approach. The research findings, obtained through simulation, further substantiate the efficacy of the proposed method, demonstrating its potential as a valuable tool for image analysis and quality control across diverse industries.

2. EXTRACTING THE FEATURES OF IMAGES

Effective use of high-volume image data can significantly improve the performance of quality monitoring methods in manufacturing and service systems. In addition, the high-density information on this type of data can provide more practical guidance in identifying the root cause of process changes and thus reduce the time it takes to return to a controlled state.

Specific features of each image are analyzed to identify differences and similarities. In digital images, pixels represent numeric values that vary based on color (black or gray). The arrangement of pixels creates a matrix with varying numbers, equal to the number of pixels in the image. Numerical calculations can be performed on pixel values, resulting in distinctive features. These features enable pattern recognition, texture recognition, and estimation of size and quantity.

An image is typically represented as a function f (x, y), where x and y are the spatial coordinates of the image, and the value at each location (x, y) is referred to as the intensity or brightness. In digital images, the intensity values are typically non-negative integers. For example, in gray images, f (x, y) can take any integer value between 0 (representing black) and 255 (representing white) for 8-bit images, or between 0 and 65,535 for 16-bit images. It should be noted that as the resolution of the image increases, the number of pixels (i.e., x, y pairs) in the image also increases, which affects the computational complexity.

This results in a much higher pixel intensity range, which can be computationally infeasible for certain applications. To address this, preset subsets called Regions of Interest (ROIs) are often used. ROIs are square-shaped regions within the image where only the mean intensities of the pixels in those regions are used as the basis for calculations, rather than examining every single pixel. This reduces the computational complexity while still providing useful information for analysis. Therefore, the kth image can be represented as a p-variate vector ((p) represents the number of windows (pROI)) based on the mean intensities of the pixels in the ROIs (Equation 1):

$$\bar{X}_{(k)} = \left(\bar{X}_{(k)}(1), \bar{X}_{(k)}(2), \dots, \bar{X}_{(k)}(p)\right) \quad (1)$$

In Phase I, the process is assumed to be in control, following a known or accurately estimated normal distribution with mean $\mu_{0.K}$ and variance ${\sigma^2}_K$. Phase II's purpose is to vigilantly monitor the process, aiming to detect specific causes that might induce a shift in the process output mean.

Control charts, encompassing Shewhart control charts and more advanced statistical process control (SPC) charts, play a pivotal role during Phase II. These charts rely on statistical methods and historical data to assess whether the current process operates within the expected range. If a specific cause leads to a shift in the process output mean, it can lead to deviations from the anticipated distribution $N(\mu_{0.K}. {\sigma^2}_K)$. The control chart promptly identifies such deviations as out-of-control signals, signaling the need for investigation and corrective actions to restore process stability. Employing control charts in Phase II is fundamental for effective process monitoring and quality control, enabling the timely mitigation of process variations to maintain quality standards.

The maximum likelihood estimates $(\hat{\mu}_1)$ and $(\hat{\tau})$ are obtained by maximizing the likelihood function over the parameter space, considering the past m images. The window of the past m images is used to capture the historical information and assess the likelihood of a mean shift based on the observed data. The generalized likelihood ratio statistic is then compared to a predefined threshold or control limits to determine if a mean shift has occurred. This statistical measure is compared to a predefined threshold or control limits to determine if a mean shift has occurred. If the generalized likelihood ratio statistic exceeds the threshold, it indicates evidence of a mean shift, and further investigation and corrective actions may be required to bring the process back under control (20):

$$R_{k,m} = \max_{0 \le \tau < k} \frac{k-\hat{\tau}_k}{2\sigma_0^2}\left(\hat{\mu}_{1,\hat{\tau}_k,k} - \mu_0\right) \quad (2)$$

It is worth mentioning that the choice of threshold or control limits for the generalized likelihood ratio statistic depends on the desired level of sensitivity and specificity in detecting mean shifts, and it may require careful consideration and validation based on the specific process and application. Additionally, the selection of the window size (m) for considering the past images also requires careful consideration to capture relevant historical information without including too much noise or irrelevant data. It is important to note that the specific values and parameters used in Equation 2, such as $k, \tau, \sigma_0, \hat{\mu}_1. \hat{\tau}_k, \mu_0$, would depend on the particular context and statistical analysis conducted in the study.

In this research, image transformations were selected to extract properties from images. Image transformations

involve transforming the revealed objects or the entire image to describe their appearance. The image features are then introduced using all or part of the transform coefficients.

While traditional methods often focus on the argument space (time or place) to extract information from signals or images, it is not always the most effective approach. In many cases, valuable information about signals or images lies in their frequency range. Mathematical transformations applied to signals or images can help to obtain this frequency-based information that may not be easily retrievable from the primary signal or image in the argument space.

The wavelet transform is a crucial tool for transforming signals or images from the argument space to the frequency space. To grasp the concept of the wavelet transform, it is essential to first comprehend the Fourier series. The Fourier series represents periodic signals or functions as a sum of various sinusoidal components with distinct frequencies and amplitudes. It is widely employed to analyze signal or image frequency content in the frequency domain.

2. 1. Frequency Domain and Fourier Transform Fourier series is a mathematical representation that expresses any periodic function as a sum of simple oscillating functions, such as sines, cosines, or mixed exponential functions. By extending a function as a Fourier series, its frequency components can be obtained, allowing for analysis of its frequency content (21).

In engineering and signal processing, functions are often defined based on time and space, as they represent various physical phenomena. Fourier transform is widely used in various areas of physics, including electronics, electromagnetics, wave physics, and geoscience, such as geophysics (22).

In Fourier transform, frequency and time information cannot be simultaneously obtained. To address this limitation, the Short-Time Fourier Transform (STFT) can be used. In the STFT, the signal's short time interval is divided into small segments, where the signal is assumed to be stationary within each segment. A window function (w) is applied to each segment, which determines the effective domain of the window function and is typically chosen to be equal to the length of the segment (23).

2. 2. Area of Location-scale and Wavelet Transform Wavelet theory, a modern addition to applied mathematics, has found widespread applications across diverse fields like seismology, signal processing, telecommunications, image processing, computer vision, genetics, medicine, criminology, and telecommunications. Wavelets, a set of mathematical functions, are instrumental in dissecting continuous signals into their frequency components, where each component's detail corresponds to its scale. This analysis leverages the wavelet transform, which breaks down a function using translated and scaled versions of a finite-length function known as the mother wavelet. A key strength of wavelet analysis is its multi-resolution nature, allowing it to extract diverse information from data at varying scales, both in the location and frequency domains simultaneously (24). The fundamental concept behind using wavelet transform for image analysis involves breaking down the image into multiple levels of detail. This process entails dividing the image into distinct domains and generating various sub-images representing different frequency components (25).

They have been used in fields such as genetics and medicine for analyzing DNA sequences, in criminology for pattern recognition in forensic analysis, and in telecommunications for signal compression and noise reduction (26). Wavelet transform $w_x(a,b)$of a continuous signal x (t) is defined in Equation 3:

$$w_x(a,b) = \frac{1}{\sqrt{a}}\int_{-\infty}^{+\infty} x(t)\psi^*(\frac{t-b}{a})dt = \big(x(t).\psi_{a.b}(t)\big) \qquad (a,b)\epsilon R^2 \tag{3}$$

In wavelet theory, the wavelet transform is obtained by multiplying the primary signal, denoted as x(t), with a translated and scaled version of a function called the mother wavelet, denoted as $\psi_{a.b}(t)$,where (a) and (b) are the scaling and translation parameters, respectively. The wavelet transform measures the similarity between the frequency content of the signal and the frequency content of the wavelet function.

The mother wavelet, ψ(t), is a function that is usually chosen to have specific properties, such as being localized in both time and frequency domains. The Haar wavelet, known for its orthogonality and symmetry, is often used for decomposing signals or images (26).

The Haar wavelet is defined in the time domain, with different values within specific intervals and 0 outside. It is piecewise constant and has compact support from 0 to 1, capturing abrupt changes in the signal.

2. 3. Wavelet-Fourier Descriptor (WFD) The Wavelet-Fourier Descriptor (WFD) is a set of coefficients obtained from Wavelet Transform (WT) of an object's signal. WT is a type of multiple resolution transform that decomposes a signal or image into different levels of detail or resolution (27). In Equation 4 the WT of an image with boundary z(t) is defined (28):

$$\mathrm{WT(a,b)} = \int \mathrm{z(t)}\psi^*\left(\mathrm{t}-\frac{\mathrm{b}}{\mathrm{a}}\right)\mathrm{dt} \tag{4}$$

where a and b are the parameters of scale and translation, respectively, ψ* is the complex conjugate of the wavelet function ψ, and z(t) is the boundary or contour of the image.

The WFD coefficients are obtained from the WT by extracting the coefficients corresponding to the limit function of the object. These coefficients represent the

frequency components of the object's signal at different scales and translations, and can be used as descriptors to characterize the object's shape or features (29). WFD is a powerful tool for image analysis and processing, as it captures the frequency information of an object's signal at different scales and translations, allowing for more detailed and accurate analysis of the object's shape, texture, and other features.

This phrase specifies wavelet coefficients on the boundary of z (t) in scale a and position b. For an optimal scale a, a set of $\mathrm{WT(a,b)}$ that is wave coefficients is obtained. WFDs are selected coefficients that are obtained based on $\mathrm{WT(a,b)}$ wave coefficients and are determined as follows in Equation 5:

$$F^a(k) = \frac{1}{N}\sum_{b=0}^{N-1} \mathrm{WT(a,b)} \exp\left(^{-j2\pi b}/_{N}\right) \quad (5)$$

It should be noted that the choice of image feature extraction technique depends on the specific requirements of the application, the type of images being analyzed, and the desired invariance properties. Each technique has its advantages and limitations, and performance evaluation should be done based on the specific criteria relevant to the application at hand [30, 31]. According to the studies, we tried to use the same advantages of both Fourier transform and wavelet.

3. SIMULATION STUDIES

The research employs the WFD algorithm for image analysis. It starts with a 250×250 pixel input image, typically a tile from a production line. The WFD algorithm combines wavelet and Fourier techniques, capturing both time and frequency information. It consists of two frequency descriptor levels: low-frequency for general characteristics and high-frequency for finer details.

The image undergoes hierarchical decomposition via recursive wavelet transforms into multiple frequency bands, resulting in a multi-scale image representation. Different bands reveal different levels of detail, enhancing image analysis (30). In this study, the Haar wavelet is specifically used for performing the wavelet transform on the image. The Haar wavelet operates by systematically replacing adjacent pairs of steps in the signal with wider steps, following a specific wavelet methodology (31).

The WFD transformation is a feature extraction technique for tile images. Key steps include:

1. Image Loading: Load a 250×250 pixel input image representing a tile from the production line.
2. Haar Wavelet Transform: Apply the Haar wavelet transform, separating the image into approximation (low-frequency) and detail (fine-detail) coefficients.
3. Fourier Transform of Wavelet Coefficients: Perform Fourier transform on wavelet coefficients, combining multi-scale representation and Fourier analysis.
4. Phase Discarding: Discard the phase part of the Fourier transform for rotation invariance, retaining magnitude information.
5. Normalization: Normalize feature vectors for scale invariance.
6. Low-Frequency and High-Frequency Descriptors: Obtain both low-frequency (general characteristics) and high-frequency (fine details) descriptors.
7. Storage of WFD Coefficients: Collect and store WFD coefficients representing combined wavelet and Fourier information.
8. Comprehensive Set of Coefficients: Repeat the process for all scales and positions to capture various image details.
9. Utilizing WFD Coefficients: Apply the obtained WFD coefficients for tasks like feature extraction, image matching, etc., benefiting from scale, rotation, and translation invariance.
10. Performance Evaluation: Assess the WFD algorithm's effectiveness in image processing tasks, considering specific criteria or metrics, e.g.

WFD transformation on tile images from the production line, it becomes possible to extract meaningful features and analyze the characteristics of the tiles in a comprehensive and invariant manner. Figure 1 represents the algorithm of the WFD technique on the input image.

The WFD algorithm applies approximation and detail coefficients recursively, capturing low-frequency components and high-frequency components with finer details (32). Figure 2 demonstrates the effectiveness of the wavelet transform, showcasing the different frequency bands obtained.

In wavelet transform, image decomposition produces distinct subbands: lowpass approximation, horizontal detail, vertical detail, and diagonal detail. The lowpass approximation represents the image's general

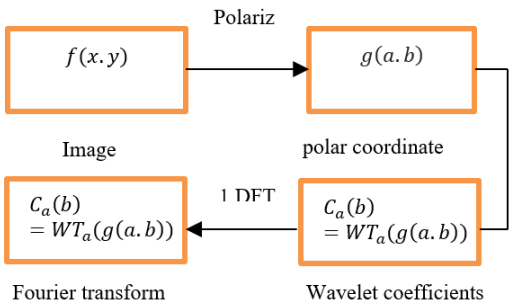

Figure 1. WFD Technique Algorithm

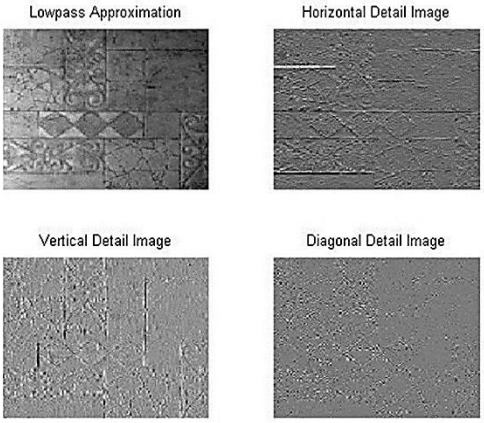

Figure 2. WFD transformation on tile image

characteristics and coarse-scale variations. The detail subbands focus on specific orientations and capture finer variations, including lines, edges, and textures. These subbands enable the analysis of the image's frequency content and spatial information at different scales (33).

This multi-scale representation is a significant advantage of using the wavelet transform in WFD algorithm.

4. CASE STUDY

First, an image of a tile obtained using an Machine Vision System (MVS) is prepared. In the next step, the received image is converted to a grayscale image. Then, we generate the actual image of the tile by subtracting the background intensity from the image. To reduce calculations, the image is resized to 250×250. Subsequently, a similar image is produced by adding noise to the image. A random noise image was added to each pixel. The random noise added to each pixel follows a Poisson distribution with a mean pixel value. In this study, the performance of the combined Wavelet-Fourier technique was thoroughly evaluated using three key criteria: average run length, standard deviation of run length, and accuracy of estimation of change point. Additionally, the size and location of faults were taken into account. The corresponding numerical results can be found in Tables 1 and 2, which provide comprehensive information regarding the performance of the technique.

To conduct the performance evaluation, the technique was tested on a total of 150 experimental fault scenarios. These scenarios encompassed a range of variables, including three fault centers, five fault sizes, and ten intensity shifts (Δ). By incorporating such diverse factors, the study aimed to thoroughly assess the effectiveness and robustness of the Wavelet-Fourier technique.

To ensure a fair comparison, the settings utilized in a previous work conducted by Megahed et al. (10) were adopted as the baseline for comparison. This allowed for a meaningful evaluation of the improvements and advancements achieved in this study.

In the pursuit of advancing our image-based quality control and monitoring methodology, a pivotal aspect of our research involves the systematic generation of controlled errors within our image dataset. These errors are meticulously designed to simulate real-world defects and anomalies in tiles, enabling us to rigorously assess the performance and robustness of our quality monitoring techniques. Figure 3, demonstrates detailed visual representation of our error generation and application process we designated in our work. The sequence of operations commences with the preparation of the image, followed by the precise creation of errors with predetermined characteristics. Subsequently, these errors are intentionally introduced into the image dataset, providing us with a controlled testbed for evaluating the efficacy of our quality control algorithms.

TABLE 1. Simulation results for 15 × 15 fault size

15*15										
$(\varepsilon_\tau) > 2$	$(\varepsilon_\tau) < -2$	$0 < (\varepsilon_\tau) \leq 2$	$(\varepsilon_\tau) = 0$	Std (ε_τ)	Med (ε_τ)	mean (ε_τ)	MRL	ARL	Δ	Fault Center
0	0	1	99	0.10	0	-0.01	1	1.11	-10	(125*125)
0	3	28	69	0.87	0	-0.17	3	3.09	-5	
9	6	36	49	1.66	0	0.17	6	6.47	-3	
54	7	25	14	12.11	3	8.35	11.50	16.18	-2	
97	1	1	1	89.79	78.50	102.96	84.50	108.97	-1	
96	1	2	1	136.50	116	149.75	123.5	154.75	1	
83	4	9	4	25.03	18	23.930	25.50	31.41	2	
24	4	32	40	3.92	0	1.9000	8	8.81	3	
2	1	25	72	1.09	0	-10.0	3	3.57	5	
0	0	0	100	0	0	0	1	1.17	10	

0	0	3	97	0.17	0	-0.03	1	1.10	-10	
0	2	21	77	0.86	0	-0.15	3	2.87	-5	
6	7	43	44	2.43	0	0.23	6	6.52	-3	
59	2	25	14	13.29	4	8.98	12	16.38	-2	
98	0	1	1	118.24	88	122.80	91	127.92	-1	(188*206)
97	0	3	0	99.57	79.50	105.02	84.50	110.68	1	
64	4	16	16	10.26	4	8.2	11	15.08	2	
19	0	33	48	1.96	0	0.90	7	6.66	3	
0	3	16	81	0.72	0	-0.10	3	2.67	5	
0	0	0	100	0	0	0	1	1.07	10	
0	1	0	99	0.80	0	-0.08	1	1.01	-10	
0	4	13	83	1.10	0	-0.26	2	2.24	-5	
3	5	34	58	1.41	0	0.17	5	4.95	-3	
46	2	29	23	7.29	2	4.87	9	11.75	-2	
92	3	3	2	63.32	47	67.91	54.50	74.14	-1	(158*78)
94	1	4	1	79.46	61	82.72	68	88.80	1	
43	4	26	27	7.06	2	4.20	10	11.46	2	
4	3	43	50	1.38	0	0.03	5	4.87	3	
0	4	10	86	1.29	0	-0.25	2	2.23	5	
0	0	0	100	0	0	0	1	1	10	

TABLE 2. Simulation results for 20 × 20 fault size

20*20										
$(\varepsilon_\tau) > 2$	$(\varepsilon_\tau) < -2$	$0 < (\varepsilon_\tau) \leq 2$	$(\varepsilon_\tau) = 0$	Std (ε_τ)	Med (ε_τ)	mean (ε_τ)	MRL	ARL	Δ	Fault Center
0	0	0	100	0	0	0	0	1	-10	
0	1	6	93	0.482	0	-0.10	2	1.56	-5	
2	2	26	70	1.147	0	-0.24	4	3.71	-3	
12	6	37	45	2.160	0	0.32	6	6.42	-2	
82	2	10	6	32.20	19	30.03	26.5	36.85	-1	(125*125)
98	1	0	1	63.30	51	67.78	57	73.57	1	
25	2	31	42	3.040	0	1.49	7	7.99	2	
3	3	32	62	1.132	0	-0.030	4	3.65	3	
0	0	6	94	0.301	0	-0.010	2	1.72	5	
0	0	0	100	0	0	0	1	1	10	
0	0	0	100	0	0	0	1	1	-10	
0	1	4	95	0.748	0	-0.080	1	1.38	-5	
1	0	18	81	0.722	0	0.060	3	3.01	-3	
9	2	37	52	2.066	0	0.340	6	5.91	-2	
77	4	10	9	39.73	17	28.24	25	35.49	-1	(188*206)
85	3	6	6	32.39	18.50	26.53	24	33.79	1	
9	2	45	44	1.664	0	0.40	5	5.62	2	
0	4	24	72	1.073	0	-0.20	3	2.81	3	
0	1	5	94	0.634	0	-0.11	1	1.43	5	
0	0	0	100	0	0	0	1	1	10	

0	0	0	100	0	0	0	1	1	-10	(158*78)
0	0	2	98	0.142	0	0	1	1.15	-5	
0	1	18	81	0.595	0	-0.10	2	2.38	-3	
2	5	24	69	1.351	0	-0.18	5	4.70	-2	
79	3	11	7	17.35	12	16.90	20	24.47	-1	
77	2	12	9	16.85	9.50	15.11	18.5	22.65	1	
2	4	33	61	1.459	0	-0.070	5	4.83	2	
0	5	6	89	1.181	0	-0.33	2	2.51	3	

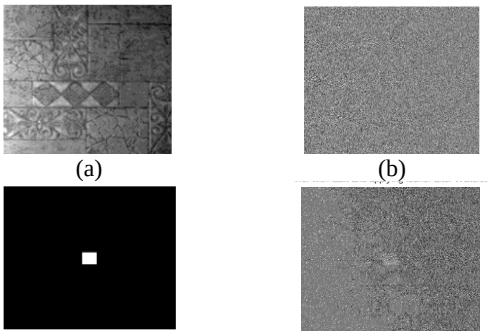

Figure 3. (a) Image, (b) Processed image, (c) Creating fault, (d) Image with fault

The study employed a sophisticated ROI production heuristic algorithm, which consisted of three distinct stages. In the first stage, grid points were strategically specified on the image based on the ratio between the number of pixels and the desired number of grid points along both the width and length dimensions. The specified ratio ranged from 25 to 100. As an example, for a 250×250 image, a ratio of 25 was selected for each direction, resulting in a total of 100 grid points evenly distributed across the entire image.

The research involved a multi-stage process to evaluate the performance of the combined Wavelet-Fourier technique in detecting faults in experimental images. In the second stage, the smallest size for ROI was determined, factoring in camera resolution, zoom level, camera position relative to the object, and image processing compression. This ensured even the smallest faults were adequately analyzed. ROIs were generated using a specific methodology, starting with the smallest size and incrementally increasing. The process continued until the image boundary was reached, following spatial guidance. The results from these ROIs were rigorously analyzed using various criteria, including average run length, standard deviation of run length, accuracy of change point estimation, and fault size and location. These criteria provided quantitative insights into the technique's effectiveness in fault detection and analysis, enabling a comprehensive evaluation of its performance.

In the second phase of the study, the proposed technique underwent rigorous evaluation using MATLAB software, primarily focusing on calculating Average Run Length (ARL) values as a performance measure. To ensure a robust assessment, the Median Run Length (MRL) criterion was also employed, offering greater reliability by being less sensitive to outliers.

To establish a reference point for the in-control condition, the ARL value was adjusted to 200, serving as a baseline for the average number of observations required to detect system faults or changes. In this evaluation, a simulation program with 1000 runs determined an MRL value of 145. This result indicates that, on average, the proposed technique detected faults at a shorter run length compared to the in-control condition, showcasing its effectiveness in prompt fault identification.

The evaluation further included comprehensive computer simulations, considering various parameters like size, quantity, and location of intensity shifts, to emulate practical fault detection scenarios. Over 1000 repetitions were performed for each parameter combination to ensure result reliability. To maintain evaluation integrity, steps were taken to mitigate environmental factors that could impact image quality, ensuring the assessment provided accurate and unbiased results.

During the comparative analysis in phase 2, the MRLvalues obtained from the simulation study were utilized. The analysis focused on assessing the proposed technique's ability to accurately detect faults when faced with different scenarios involving variations in fault size, quantity, and location of intensity shifts.

By thoroughly examining the results obtained from the simulation study, a comprehensive understanding of the proposed technique's performance was achieved. The analysis provided insights into the technique's effectiveness in detecting faults across a range of conditions, allowing researchers and readers to gain valuable knowledge about its capabilities and limitations. This rigorous evaluation process ensured that the proposed technique's performance was thoroughly assessed and its ability to detect faults under diverse conditions was accurately characterized.In this study,

several factors were considered to conduct a comprehensive case study analysis. The size of the smallest ROI was determined to be 22×22 pixels, providing a baseline for evaluating the proposed method's performance. Three defect centers were selected at coordinates (188×206), (78×158), and (125×125), representing different positions within the image. These defect centers were analyzed to assess the effectiveness of the proposed method in detecting faults. Upon analyzing the results for the mentioned defect centers, it was observed that the proposed method demonstrated superior performance for the centers at (188×206) and (78×158). However, the results for the center at (125×125) were comparable to previous studies, indicating that the proposed method can yield similar outcomes in such cases. This finding suggests that employing combined methods of image extraction allows for a more comprehensive investigation of different areas within the image. Additionally, statistics such as the change point ($\varepsilon_\tau = \hat{\tau} - \tau$) were reported in the Table. Change point analysis is a statistical technique used in process monitoring to identify significant shifts or changes in a process's behavior. It helps detect sudden variations in process parameters or quality measurements, highlighting potential alterations in process dynamics or operating conditions. Change point analysis is a valuable tool for monitoring processes, enabling timely interventions, quality improvements, and waste reduction. However, it requires careful consideration of data quality, appropriate statistical methods, and interpretation of results in the context of the specific process being monitored. For example, in the case of a fault size of 15×15 at the center of a 206×188 image, with a $\Delta = -3$, the average run length is 6. Conversely, for a fault size of 20×20 with the same specifications, it is reduced to 3. A noteworthy point to consider is that both of these defect sizes are smaller than the smallest window. Additionally, it can be claimed that larger defect sizes are detected more quickly.

In accordance with Megahed et al.'s (10) work, the proposed change point technique demonstrated generally robust performance across various fault sizes. However, similar studies have indicated a notable decrease in performance when dealing with minor intensity shifts and fault sizes of 15×15 pixels or smaller. This aligns with expectations, as tiny intensity shifts can be challenging to precisely diagnose, particularly when barely perceptible to the human eye. The study revealed that the proposed method excelled in detecting faults within the range of intensity shifts from -10 to 10, irrespective of the defect size. This highlights the method's effectiveness in identifying faults within this specific intensity shift range. Table 3 presents a comparative analysis between this study's results and Megahed et al.'s (10) work, with a focus on a 15×15 pixel fault centered at (125×125). The findings indicate that the proposed method performs notably better for faults situated at the sides or edges of the image or ROI. This underscores the approach's particular efficacy in detecting faults in these peripheral areas.

An essential observation from the analysis pertains to the relationship between the size of the smallest ROI and the minimum fault size requiring identification. Properly sizing and positioning the ROI in relation to the fault size are critical considerations that significantly influence detection accuracy and reliability. Overlapping between the ROI and the fault can introduce complexities and potentially compromise detection accuracy. This emphasizes the need for meticulous attention to ROI design and positioning to ensure precise fault detection. Addressing the potential impact of overlapping factors on detection accuracy is crucial for enhancing fault detection techniques' effectiveness and overall accuracy in fault identification. The comparison in Table 3 not only highlights the superior performance of the proposed method for peripheral faults but also underscores the critical importance of appropriately sizing and positioning the ROI to mitigate overlapping factors that may affect detection accuracy. These insights provide valuable guidance for future research in fault detection, emphasizing the need for meticulous ROI design and positioning consideration.

The Dice Similarity Coefficient (DSC) calculates the spatial overlap between the target areas A and B. It provides a numerical value ranging from 0 to 1, where a value of 1 indicates perfect agreement or complete overlap between the target areas, while a value of 0 represents no overlap or similarity (34). The DSC is calculated using Equation 6 mentioned in the study. This information is crucial in determining the reliability and effectiveness of the method for fault localization and provides insights into the potential applications and performance of the proposed technique (34).

$$\mathrm{DSC}\,(\mathrm{A}\,,\mathrm{B}\,) = \frac{(2\times|A\cap B|)}{|A|+|B|} \quad (6)$$

In the realm of fault detection and localization, the DSC serves as a crucial evaluation metric for assessing the accuracy and congruence between estimated and reference fault locations. A higher DSC value signifies more precise fault estimation, while a lower value implies reduced accuracy. To enhance the assessment, two additional metrics, the Median of Dice Similarity Coefficient (MDSC) and the Maximum Achievable Dice Similarity Coefficient (MADSC), are employed. MDSC offers a benchmark for gauging typical similarity between estimated and actual fault areas, independent of heuristic techniques for generating ROI. Meanwhile, MADSC quantifies the upper limit of attainable similarity, acting as a reference point, especially for specific fault sizes. The incorporation of MDSC and MADSC enables a comprehensive evaluation of the method's precision in fault size and location estimation,

shedding light on its potential and limitations within the given conditions. In essence, these measures enrich the assessment of the proposed method's fault estimation performance.

For example, for faults of size 20×20, MADSC is calculated as follows:

$$\frac{(2*|20*20|)}{|20*20|+|(22*22)|} = 0.905$$

Table 4 showcases the performance of the method in estimating the time and size of faults under intensity shifts. To evaluate the method's performance, the ratio of $\left(\frac{MDSC}{MADSC}\right)$ is employed as a measure. This ratio serves as an indicator of how well the method performs compared to the maximum achievable similarity between the estimated and actual fault areas. It is important to note that this assessment assumes alignment between the ROI center and the fault of the MADSC benchmark structure.

The ratio is calculated for all three fault centers considered in the study. For the two side centers, where the intensity shifts are high, the ratio is predominantly above 0.5. This suggests that the method performs relatively well in these scenarios, exhibiting satisfactory performance in estimating both the time and size of faults.

Similarly, for the center located at (125×125) with faults larger than the smallest ROI, the ratio is higher than 0.5, indicating a favorable performance. However, it is worth noting that cases where |Δ|=1 and the fault size is 10x10 might result in an MDSC value of 0. This is expected because the MRL value in these cases is very close to the MRL under control conditions. Consequently, most of these signals are likely to be false alerts attributed to the shift, leading to a lower coverage benchmark.

In summary, Table 4 provides insights into the method's performance in estimating the time and size of faults under intensity shifts. The ratio of MDSC to MADSC serves as a comparative measure, showcasing the method's performance relative to the maximum achievable similarity. The observed results indicate favorable performance for faults located at the side centers and for larger faults at the center (125×125). However, it is important to consider the specific conditions and limitations, as cases with minimal intensity shifts and smaller fault sizes may yield lower MDSC values due to potential false alerts.

5. MANAGEMENT INSIGHT

In the contemporary data-driven landscape, extracting insights from abundant image data is pivotal for manufacturing and service systems. This insight offers a practical roadmap for applying the proposed method:

TABLE 3. Comparison with other research for size faults 15*15

Proposed method								15*15
$(\varepsilon_\tau) > 2$	$(\varepsilon_\tau) < -2$	$0 < (\varepsilon_\tau) \leq 2$	$(\varepsilon_\tau) = 0$	Std (ε_τ)	Med (ε_τ)	mean (ε_τ)	Δ	Fault Center
0	3	28	69	0.87	0	-0.17	-5	
9	6	36	49	1.66	0	0.17	-3	
54	7	25	14	12.11	3	8.35	-2	
97	1	1	1	89.79	78.50	102.96	-1	(125*125)
96	1	2	1	136.50	116	149.75	1	
83	4	9	4	25.03	18	23.930	2	
24	4	32	40	3.92	0	1.9000	3	
2	1	25	72	1.09	0	-10.0	5	
Research by Megahed et al. [10]								
0.3	2.2	20.5	77	0	0.851	-0.095	-5	
16.6	3.1	36.8	43.5	0	2.623	0.912	-3	
72.3	2.1	15.7	9.9	9	16.577	13.795	-2	
96.9	0.7	1.7	0.7	83	131.78	126.02	-1	(125*125)
96.6	0.5	2.3	0.6	87.5	123.56	124.44	1	
71.3	1.2	17.5	10	8.5	15.085	12.735	2	
14.6	3.5	38.2	43.7	0	2.461	0.821	3	
0.4	2.4	18	79.2	0	0.875	-0.099	5	

Step 1: Introduction and Context
Highlighting the relevance, this approach underscores the importance of using image data for quality monitoring and process control. It recognizes the need for robust methods in an era of data abundance.
Step 2: Selecting the Most Suitable Method
Emphasizing method selection, the insight advocates the Wavelet-Fourier approach's superiority over individual methods like Fourier or Wavelet transforms. This underscores the critical role of choosing optimal feature extraction methods for effective online process monitoring.
Step 3: Identifying Image Processing Issues and Providing Valuable Information
Underlining the method's capability to identify image processing issues, it emphasizes its ability to estimate change points, fault locations, and sizes. This empowers organizations to promptly address process changes, reducing downtime
Step 4: Integration of Image Data Analysis into Quality Monitoring
Highlighting the potential of integrating image data analysis into quality monitoring, it showcases the profound insights that dense image data can provide, leading to enhanced decision-making, efficiency, cost savings, and customer satisfaction.
Step 5: Conclusion and Overall Benefit
Reiterating the overarching benefits, it underscores how effective image data utilization and advanced feature extraction methods can improve quality monitoring, drive efficiency, reduce costs, and elevate customer satisfaction in today's competitive business landscape.

TABLE 4. Comparison of (MDSC/MADSC) for all 3 fault centers & 10 values intensity shift

	(78*158)				**(188*206)**			**(125*125)**		
Δ	size	E	Med	$\frac{MDSC}{MADSC}$	E	Med	$\frac{MDSC}{MADSC}$	E	Med	$\frac{\boldsymbol{MDSC}}{\boldsymbol{MADSC}}$
-10	10*10	0.155	0.163	0.477	0.165	0.180	0.524	0.193	0.224	**0.652**
	15*15	0.242	0.243	0.383	0.265	0.270	0.425	0.336	0.368	**0.580**
	20*20	0.334	0.333	0.368	0.371	0.367	0.405	0.424	0.454	**0.501**
	30*30	0.475	0.482	0.482	0.579	0.581	0.581	0.556	0.596	**0.596**
	50*50	0.629	0.632	0.632	0.764	0.765	0.765	0.670	0.658	**0.658**
-5	10*10	0.146	0.149	0.433	0.143	0.163	0.477	0.170	0.224	**0.652**
	15*15	0.230	0.243	0.383	0.259	0.270	0.425	0.308	0.346	**0.545**
	20*20	0.321	0.333	0.368	0.374	0.385	0.426	0.394	0.428	**0.473**
	30*30	0.460	0.467	0.467	0.562	0.581	0.581	0.538	0.553	**0.553**
	50*50	0.624	0.623	0.623	0.755	0.765	0.765	0.685	0.658	**0.658**
-3	10*10	0.122	0.147	0.430	0.114	0.147	0.430	0.140	0.127	**0.370**
	15*15	0.225	0.243	0.383	0.253	0.270	0.425	0.302	0.346	**0.544**
	20*20	0.309	0.333	0.368	0.372	0.389	0.430	0.394	0.428	**0.473**
	30*30	0.450	0.467	0.467	0.537	0.551	0.551	0.499	0.521	**0.521**
	50*50	0.610	0.620	0.620	0.742	0.745	0.745	0.673	0.658	**0.658**
-2	10*10	0.068	0.024	0.071	0.048	0	0	0.084	0.038	**0.111**
	15*15	0.199	0.243	0.383	0.219	0.270	0.425	0.275	0.346	**0.544**
	20*20	0.300	0.333	0.368	0.349	0.389	0.430	0.366	0.403	**0.445**
	30*30	0.427	0.448	0.448	0.518	0.552	0.552	0.494	0.502	**0.502**
	50*50	0.570	0.605	0.605	0.725	0.725	0.725	0.673	0.658	**0.658**
-1	10*10	0.022	0	0	0.009	0	0	0.0149	0	**0**
	15*15	0.102	0.060	0.94	0.089	0	0	0.131	0.101	**0.159**
	20*20	0.242	0.320	0.345	0.241	0.333	0.368	0.297	0.307	**0.339**
	30*30	0.385	0.433	0.433	0.510	0.543	0.543	0.478	0.502	**0.502**
	50*50	0.561	0.588	0.588	0.695	0.732	0.732	0.616	0.652	**0.652**

1	10*10	0.011	0	0	0.0127	0	0	0.0183	0	**0**
	15*15	0.050	0	0	0.113	0.066	0.104	0.158	0.121	**0.191**
	20*20	0.167	0.173	0.191	0.275	0.365	0.404	0.303	0.321	**0.355**
	30*30	0.389	0.443	0.443	0.526	0.559	0.559	0.479	0.585	**0.585**
	50*50	0.567	0.594	0.594	0.694	0.723	0.723	0.632	0.652	**0.652**
2	10*10	0.029	0	0	0.067	0.030	0.086	0.0861	0.063	**0.184**
	15*15	0.198	0.243	0.383	0.206	0.270	0.425	0.275	0.346	**0.544**
	20*20	0.298	0.332	0.367	0.361	0.381	0.422	0.348	0.331	**0.367**
	30*30	0.442	0.456	0.456	0.531	0.551	0.551	0.502	0.540	**0.540**
	50*50	0.582	0.610	0.610	0.723	0.743	0.743	0.665	0.658	**0.658**
3	10*10	0.081	0.089	0.259	0.110	0.147	0.430	0.149	0.134	**0.390**
	15*15	0.223	0.243	0.383	0.247	0.270	0.425	0.306	0.346	**0.544**
	20*20	0.312	0.333	0.368	0.360	0.378	0.418	0.380	0.421	**0.465**
	30*30	0.447	0.467	0.467	0.464	0.575	0.575	0.514	0.540	**0.540**
	50*50	0.608	0.618	0.618	0.748	0.765	0.765	0.682	0.681	**0.681**
5	10*10	0.140	0.147	0.430	0.0154	0.163	0.477	0.164	0.202	**0.588**
	15*15	0.230	0.243	0.383	0.259	0.270	0.425	0.315	0.346	**0.544**
	20*20	0.320	0.333	0.368	0.361	0.378	0.418	0.398	0.428	**0.473**
	30*30	0.462	0.467	0.467	0.563	0.581	0.581	0.535	0.540	**0.540**
	50*50	0.620	0.623	0.623	0.759	0.765	0.765	0.683	0.658	**0.658**
10	10*10	0.154	0.163	0.477	0.157	0.163	0.477	0.195	0.334	**0.652**
	15*15	0.239	0.243	0.383	0.261	0.270	0.425	0.333	0.368	**0.580**
	20*20	0.333	0.33	0.368	0.375	0.367	0.405	0.425	0.454	**0.501**
	30*30	0.475	0.482	0.482	0.577	0.581	0.581	0.567	0.596	**0.596**
	50*50	0.630	0.634	0.634	0.764	0.765	0.765	0.690	0.658	**0.658**

By following these steps, the management insight provides a clear and concise overview of the research findings and their implications for management in manufacturing and service systems.

It highlights the importance of selecting the right method, the benefits of identifying image processing issues, and the value of integrating image data analysis into quality monitoring practices.

6. CONCLUSION

This study has successfully demonstrated the effectiveness of the combined Wavelet-Fourier technique for enhancing fault detection in image analysis for fabrication quality control. The proposed approach not only identifies image processing issues but also provides valuable information for estimating change points, fault locations, and sizes, leading to more efficient resolution and prediction of faults. Through the evaluation of its performance on experimental images, the combined Wavelet-Fourier technique showcased reliable fault detection capabilities, outperforming existing methods, particularly for faults situated at the edges or sides of the image. The comprehensive analysis of evaluation criteria and benchmark measures confirmed the method's superior performance, signifying its potential for diverse applications in manufacturing and quality control. By leveraging image data for statistical process control, manufacturers can make informed decisions to improve overall product quality while achieving cost and time savings in production. The practical implications of this research extend beyond the laboratory, offering a comprehensive solution for fault detection and analysis in various industries. Proper consideration and adjustment of parameters, such as the size and positioning of the region of interest, are crucial to obtaining accurate fault detection results. While the results are promising, it's essential to acknowledge certain limitations and suggest avenues for future research. One limitation of our study is the sensitivity of the proposed method to parameter

settings, such as the size and positioning of the ROI. Further investigation into parameter robustness and automated parameter optimization methods could enhance the technique's applicability. The experimental dataset primarily focused on specific fault scenarios. Future research should expand the scope to include a more diverse range of fault types and complexities to validate the method's effectiveness across various industrial applications. Also continued research should aim to refine and optimize the combined Wavelet-Fourier technique. This includes exploring variations of the method and fine-tuning its parameters to make it more adaptable to different image datasets and fault scenarios. Future studies should consider applying the technique to a broader range of image datasets from various industries. This will help assess its versatility and generalizability in different manufacturing and service systems. Investigate the integration of automated parameter tuning and machine learning algorithms to enhance the method's efficiency and accuracy in fault detection, potentially enabling real-time implementation. In summary, while the combined Wavelet-Fourier technique represents a significant advancement in fault detection, addressing its limitations and pursuing further research avenues will be instrumental in harnessing its full potential for the benefit of manufacturing and quality control across diverse industries.

7. REFERENCES

1. Feng J, Fu J, Lin Z, Shang C, Li B. A review of the design methods of complex topology structures for 3D printing. Visual Computing for Industry, Biomedicine, and Art. 2018;1(1):1-16. https://doi.org/10.1186/s42492-018-0004-3
2. Hu G-H, Wang Q-H, Zhang G-H. Unsupervised defect detection in textiles based on Fourier analysis and wavelet shrinkage. Applied optics. 2015;54(10):2963-80. https://doi.org/10.1364/AO.54.002963
3. Zahn CT, Roskies RZ. Fourier descriptors for plane closed curves. IEEE Transactions on computers. 1972;100(3):269-81. https://doi.org/10.1109/TC.1972.5008949
4. Chen G, Bui TD. Invariant Fourier-wavelet descriptor for pattern recognition. Pattern recognition. 1999;32(7):1083-8. https://doi.org/10.1016/S0031-3203(98)00148-4
5. Liu JJ, MacGregor JF. Estimation and monitoring of product aesthetics: application to manufacturing of "engineered stone" countertops. Machine Vision and Applications. 2006;16:374-83. https://doi.org/10.1007/s00138-005-0009-8
6. Yadav RB, Nishchal NK, Gupta AK, Rastogi VK. Retrieval and classification of shape-based objects using Fourier, generic Fourier, and wavelet-Fourier descriptors technique: A comparative study. Optics and Lasers in engineering. 2007;45(6):695-708. https://doi.org/10.1016/j.optlaseng.2006.11.001
7. Hosntalab M, Aghaeizadeh Zoroofi R, Abbaspour Tehrani-Fard A, Shirani G. Classification and numbering of teeth in multi-slice CT images using wavelet-Fourier descriptor. International journal of computer assisted radiology and surgery. 2010;5:237-49. https://doi.org/10.1007/s11548-009-0389-8
8. Münch B, Trtik P, Marone F, Stampanoni M. Stripe and ring artifact removal with combined wavelet—Fourier filtering. Optics express. 2009;17(10):8567-91. https://doi.org/10.1364/OE.17.008567
9. Ward M, Xie Z, Yang D, Rundensteiner E. Quality-aware visual data analysis. Computational Statistics. 2011;26(4):567-84. https://doi.org/10.1007/s00180-010-0226-0
10. Megahed FM, Wells LJ, Camelio JA, Woodall WH. A spatiotemporal method for the monitoring of image data. Quality and Reliability Engineering International. 2012;28(8):967-80. https://doi.org/10.1002/qre.1287
11. Chen G, Xie W, Bui TD, Krzyżak A. Automatic epileptic seizure detection in EEG using nonsubsampled wavelet–fourier features. Journal of Medical and Biological Engineering. 2017;37:123-31. https://doi.org/10.1007/s40846-016-0214-0
12. Knešaurek K. Fourier-wavelet restoration in PET/CT brain studies. Nuclear Instruments and Methods in Physics Research Section A: Accelerators, Spectrometers, Detectors and Associated Equipment. 2012;689:29-34. https://doi.org/10.1016/j.nima.2012.06.032
13. Xia Y, Johnson BK, Jiang Y, Fischer N, Xia H. A new method based on artificial neural network, Wavelet Transform and Short Time Fourier Transform for Subsynchronous Resonance detection. International Journal of Electrical Power & Energy Systems. 2018;103:377-83. https://doi.org/10.1016/j.ijepes.2018.06.019
14. Al-Salman W, Li Y, Wen P. Detecting sleep spindles in EEGs using wavelet fourier analysis and statistical features. Biomedical Signal Processing and Control. 2019;48:80-92. https://doi.org/10.1016/j.bspc.2018.10.004
15. You L, Man J, Yan K, Wang D, Li H. Combined Fourier-wavelet transforms for studying dynamic response of anisotropic multi-layered flexible pavement with linear-gradual interlayers. Applied Mathematical Modelling. 2020;81:559-81. https://doi.org/10.1016/j.apm.2020.01.031
16. Biglari M, Mirzaei F, Hassanpour H. Feature selection for small sample sets with high dimensional data using heuristic hybrid approach. International Journal of Engineering, Transactions B: Applications. 2020;33(2):213-20. https://doi.org/10.5829/IJE.2020.33.02B.05
17. Fattahzadeh M, Saghaei A. A statistical method for sequential images–based process monitoring. International Journal of Engineering, Transactions A: Basics. 2020;33(7):1285-92. https://doi.org/10.5829/IJE.2020.33.07A.15
18. Santosh NK, Barpanda SS. Wavelet and PCA-based glaucoma classification through novel methodological enhanced retinal images. Machine Vision and Applications. 2022;33(1):11. https://doi.org/10.1007/s00138-021-01263-w
19. Abdul-Kareem AA, & Al-Jawher, W. A. M. . A Hybrid Domain Medical Image Encryption Scheme Using URUK and WAM Chaotic Maps with Wavelet–Fourier Transform. Journal of Cyber Security and Mobility. 2023:435-64.
20. Reynolds Jr MR, Lou J. An evaluation of a GLR control chart for monitoring the process mean. Journal of quality technology. 2010;42(3):287-310. https://doi.org/10.1080/00224065.2010.11917825
21. Wirsing K. Time frequency analysis of wavelet and Fourier transform. Wavelet theory. 2020.
22. Stein EM, Weiss G. Introduction to Fourier Analysis on Euclidean Spaces (PMS-32). Introduction to Fourier Analysis on Euclidean Spaces (PMS-32).32.
23. Zhang Z, Jing Z, Wang Z, Kuang D. Comparison of Fourier transform, windowed Fourier transform, and wavelet transform

methods for phase calculation at discontinuities in fringe projection profilometry. Optics and Lasers in Engineering. 2012;50(8):1152-60. https://doi.org/10.1016/j.optlaseng.2012.03.004

24. Lin L, Feng L. Comparative analysis of image denoising methods based on wavelet transform and threshold functions. International Journal of Engineering. 2017;30(2):199-206. https://doi.org/10.5829/idosi.ije.2017.30.02b.06
25. Kunttu I, Lepistö L, Rauhamaa J, Visa A. Multiscale Fourier descriptors for defect image retrieval. Pattern Recognition Letters. 2006;27(2):123-32. https://doi.org/10.1016/j.patrec.2005.08.022
26. Mallat S. A wavelet tour of signal processing: Elsevier; 1999.
27. Shen D IH. Discriminative wavelet shape descriptors for recognition of 2-D patterns. Pattern recognition. 1999;32(2):151-65.
28. Illanes A, Esmaeili N, Poudel P, Balakrishnan S, Friebe M. Parametrical modelling for texture characterization—A novel approach applied to ultrasound thyroid segmentation. PloS one. 2019;14(1):e0211215. https://doi.org/10.1371/journal.pone.0211215
29. Matuszewski DJ, Hast A, Wählby C, Sintorn I-M. A short feature vector for image matching: The Log-Polar Magnitude feature descriptor. Plos one. 2017;12(11):e0188496. https://doi.org/10.1371/journal.pone.0188496
30. Bishop CM, Nasrabadi NM. Pattern recognition and machine learning: Springer; 2006.
31. Rao RM. Wavelet transforms: Introduction to theory and applications: Pearson Education India; 1998.
32. Haar A. Zur theorie der orthogonalen funktionensysteme: Georg-August-Universitat, Gottingen.; 1909.
33. Kumar S, Bhandari AK, Raj A, Swaraj K. Triple clipped histogram-based medical image enhancement using spatial frequency. IEEE Transactions on NanoBioscience. 2021;20(3):278-86. https://doi.org/10.1109/TNB.2021.3064077
34. Wang J, Cui L, Xu Y. Quantitative and localization fault diagnosis method of rolling bearing based on quantitative mapping model. Entropy. 2018;20(7):510. https://doi.org/10.3390/e20070510

Persian Abstract

چکیده

این مطالعه بر استفاده از داده‌های تصویری برای کنترل فرآیند آماری و بهبود نظارت بر کیفیت در سیستم‌های تولید و خدمات تمرکز دارد. اثربخشی روش‌های استخراج ویژگی فردی و ترکیبی با رویکرد موجک- فوریه به عنوان مناسب‌ترین روش مورد ارزیابی قرار می‌گیرد. روش پیشنهادی نه تنها مسائل مربوط به پردازش تصویر را شناسایی می‌کند، بلکه اطلاعات ارزشمندی را برای تخمین نقاط تغییر، مکان‌های خطا و اندازه خطا ارائه می‌دهد. این امکان حل و پیش بینی خطا را فراهم می کند و منجر به صرفه جویی در هزینه و زمان در تولید می شود. برای ارزیابی عملکرد روش، تصویری از خط تولید کاشی تحت تبدیل موجک قرار می‌گیرد و به دنبال آن تبدیل فوریه روی ضرایب به‌دست‌آمده انجام می شود. نتایج نشان دهنده برتری روش موجک- فوریه بر روش های فردی مانند تبدیل فوریه و تبدیل موجک است. روش پیشنهادی، عملکرد قابل مقایسه یا بهبود یافته ای را در تشخیص و مکان خطا در مقایسه با تحقیقات مشابه نشان می دهد. این مطالعه پتانسیل استفاده از داده های تصویری برای کنترل فرآیند آماری و نظارت بر کیفیت را برجسته می کند و راه حلی جامع برای تشخیص و تجزیه و تحلیل خطا ارائه می دهد. این یافته ها به پیشرفت در تکنیک های پردازش تصویر کمک می کند و پیامدهای عملی برای افزایش نظارت بر کیفیت در صنایع مختلف دارد. با استفاده از داده‌های تصویر، تولیدکنندگان می‌توانند تصمیمات آگاهانه بگیرند، عملکرد فرآیند را افزایش دهند و کیفیت کلی محصول را بهبود بخشند.